BNL-99215-2013-TECH
C-A/AP/62;BNL-99215-2013-IR

Analytical Field Calculation of Helical Magnets with an Axilly Symmetric Iron Yoke

T. Tominaka

September 2001

Collider Accelerator Department
Brookhaven National Laboratory

U.S. Department of Energy
USDOE Office of Science (SC)

DISCLAIMER

C-A/AP/62
September 2001

Analytical Field Calculation of Helical Magnets with an Axially Symmetric Iron Yoke

T. Tominaka, M. Okamura, & T. Katayama

Collider-Accelerator Department
Brookhaven National Laboratory
Upton, NY 11973

Final manuscript to NIM-A

Analytical Field Calculation of Helical Magnets with an Axially Symmetric Iron Yoke

T. Tominaka[a,*,1], M. Okamura[a], and T. Katayama[a,b]

[a]RIKEN (The Institute of Physical and Chemical Research),
2-1, Hirosawa, Wako, Saitama, 351-0198, Japan

[b]Center for Nuclear Study, School of Science, University of Tokyo,
RIKEN, 2-1, Hirosawa, Wako, Saitama, 351-0198, Japan

Abstract

The magnetic field due to a current flowing in a helical conductor placed inside a cylindrical hole in iron is investigated. In order to calculate the contribution of an axially symmetric iron yoke on the inner field of helical magnets, a 3-dimensional potential problem is solved. The obtained analytical expressions are applied for the helical dipole magnet for the Relativistic Heavy Ion Collider (RHIC), with good agreement.

Keywords : Magnetic Fields; Superconducting magnets; Magnetization; Accelerators; Polarized beams; Brookhaven RHIC

1 INTRODUCTION

The analytical expressions of the magnetic fields due to a single straight current inside a hollow iron yoke whose inner surface is a cylinder is basically applied for the calculation of the two-dimensional (2D) magnetic fields due to a long superconducting dipole for a large accelerator. In this 2D magnet, it is revealed that the effect of iron on the inner field can be calculated with the method of an image current if the iron is not saturated and the permeability is uniform.

In this paper, the contribution of an axially symmetric iron yoke on the helical magnets is studied, on the base of the analytical expressions of the magnetic fields due to a single helical current. [1] The results obtained from the assumption of a helical image current have some disagreements for the other numerical calculation and measured results. [1]

In order to obtain the rigorous expressions for the contribution of an axially symmetric iron yoke without saturation on the interior field of helical magnets, a 3-dimensional

* Corresponding author.
E-mail address:tominaka@postman.riken.go.jp (T. Tominaka).

[1] Permanent address: Hitachi Research Laboratory, Hitachi, Ltd., 1-1, 7-chome, Omika-cho, Hitachi, Ibaraki, 319-1292, Japan.

potential problem is solved. Then, the calculation of the interior field of the helical dipole magnet for RHIC is corrected by using the obtained analytical expressions.

2 FIELD OF A SINGLE HELICAL CURRENT CONDUCTOR

In this paper, the magnetic induction B, the magnetic scalar potential ϕ_m and the vector potential A are defined as follows,

$$B = -\mu\nabla\phi_m = \nabla \times A \tag{1}$$

Similarly, the relation between the magnetic induction B, and the magnetic field intensity H is defined as follows,

$$B = \mu_0(H+M) = \mu_0(1+\chi_m)H = \mu_0\kappa_m H = \mu H \tag{2}$$

where μ is the absolute permeability, χ_m is the magnetic susceptibility, and κ_m is the relative permeability.

On the case that a single helical current carrying conductor with a pitch length L (= $2\pi/k$) is located at some point (r=b, $\theta=\varphi$) at the z=0 plane, as shown in Figs. 1 and 2, the magnetic scalar potential ϕ_m and the field B due to a single helical current carrying conductor without iron are written in the following forms, [1]
for r < b,

$$\phi_m(r,\theta,z) = -\frac{I}{2\pi}kz - \frac{I}{\pi}kb\sum_{n=1}^{\infty}K_n'(nkb)I_n(nkr)\sin[n(\theta-\varphi-kz)] \tag{3}$$

$$\begin{cases} B_r(r,\theta,z) = \dfrac{\mu_0 I}{\pi}k^2 b\sum\limits_{n=1}^{\infty}nK_n'(nkb)I_n'(nkr)\sin[n(\theta-\varphi-kz)] \\ B_\theta(r,\theta,z) = \dfrac{\mu_0 I}{\pi}kb\sum\limits_{n=1}^{\infty}nK_n'(nkb)\dfrac{I_n(nkr)}{r}\cos[n(\theta-\varphi-kz)] \\ B_z(r,\theta,z) = \dfrac{\mu_0 I}{2\pi}k - \dfrac{\mu_0 I}{\pi}k^2 b\sum\limits_{n=1}^{\infty}nK_n'(nkb)I_n(nkr)\cos[n(\theta-\varphi-kz)] \end{cases} \tag{4}$$

Similarly, for r > b,

$$\phi_m(r,\theta,z) = -\frac{I}{2\pi}\theta - \frac{I}{\pi}kb\sum_{n=1}^{\infty} I_n'(nkb)K_n(nkr)\sin[n(\theta-\varphi-kz)] \tag{5}$$

$$\begin{cases} B_r(r,\theta,z) = \dfrac{\mu_0 I}{\pi}k^2 b\sum_{n=1}^{\infty} nI_n'(nkb)K_n'(nkr)\sin[n(\theta-\varphi-kz)] \\ B_\theta(r,\theta,z) = \dfrac{\mu_0 I}{2\pi r} + \dfrac{\mu_0 I}{\pi}kb\sum_{n=1}^{\infty} nI_n'(nkb)\dfrac{K_n(nkr)}{r}\cos[n(\theta-\varphi-kz)] \\ B_z(r,\theta,z) = -\dfrac{\mu_0 I}{\pi}k^2 b\sum_{n=1}^{\infty} nI_n'(nkb)K_n(nkr)\cos[n(\theta-\varphi-kz)] \end{cases} \tag{6}$$

3 3-DIMENSIONAL POTENTIAL PROBLEM OF HELICAL MAGNETS

On the case that a single helical current conductor with a pitch length L (= $2\pi/k$) is located at some point (r=b, θ=0) in the z=0 plane placed inside a cylindrical hole in iron of $\mu_2 = \kappa_m\mu_0$, as shown in Figs. 1 and 2, the general form for the magnetic scalar potential ϕ_1 of regions 1, (r < a) is expressed as a sum of the contribution $\phi_{1,coil}$ of a single helical current conductor and the contribution $\phi_{1,iron}$ of an axially symmetric iron yoke in the following from,

$$\phi_1(r,\theta,z) = \phi_{1,coil}(r,\theta,z) + \phi_{1,iron}(r,\theta,z) \tag{7}$$

Furthermore, the magnetic scalar potential due to a single helical current conductor is expressed by Eq.(3) for the interior region of the helical coil (r < b) or Eq.(5) for the exterior region of the helical coil (b < r < a).

Since the terms of the modified Bessel function of the second kind, $K_n(nkr)$ are excluded by the condition that the origin be a regular point for the contribution of iron, the general solutions at z=0 for the magnetic scalar potential ϕ_1 and ϕ_2 of both regions can be written in the following forms with the unknown constants of A_n, B_0, and B_n,
for b < r < a,

$$\phi_1(r,\theta,z=0) = -\frac{I}{2\pi}\theta - \frac{I}{\pi}kb\sum_{n=1}^{\infty} I_n'(nkb)K_n(nkr)\sin n\theta - \frac{I}{\pi}\sum_{n=1}^{\infty} A_n I_n(nkr)\sin n\theta \tag{8}$$

similarly, for r > a,

$$\phi_2(r,\theta,z=0) = -\frac{I}{2\pi}B_0\theta - \frac{I}{\pi}\sum_{n=1}^{\infty}B_nK_n(nkr)\sin n\theta \tag{9}$$

The constants may be determined by the use of the boundary conditions on the interface, r = a, between regions 1, (r < a) and 2, (r > a). On the boundary between the region 1 ($\mu_1 = \mu_0$) and the region 2 ($\mu_2 = \kappa_m\mu_0$), the following conditions must be fulfilled,

$$\begin{cases} H_{t1} = H_{t2} \\ B_{n1} = B_{n2} \end{cases} \tag{10}$$

The continuity of the tangential component of H at the boundary r = a is equivalent to the continuity of ϕ_m, while the continuity of the normal component of B demands that

$$\mu_1\frac{\partial\phi_1}{\partial r} = \mu_2\frac{\partial\phi_2}{\partial r}$$

at r = a. Then, the above boundary conditions are equivalent with the following condition for the magnetic scalar potential.

$$\begin{cases} \phi_1 = \phi_2 \\ \mu_1\dfrac{\partial\phi_1}{\partial r} = \mu_2\dfrac{\partial\phi_2}{\partial r} \end{cases} \tag{11}$$

From the first condition of Eq. (11), the following relations are obtained,

$$\begin{cases} kbI_n'(nkb)K_n(nka) + A_nI_n(nka) = B_nK_n(nka) \\ B_0 = 1 \end{cases} \tag{12}$$

Similarly, from the second condition of Eq. (11), the following relation is obtained,

$$kbI_n'(nkb)K_n'(nka) + A_nI_n'(nka) = \kappa_mB_nK_n'(nka) \tag{13}$$

From Eqs.(12) and (13), the unknown constants are determined as follows,

$$A_n = -kb\frac{(\kappa_m - 1)K_n(nka)K_n'(nka)}{\kappa_mI_n(nka)K_n'(nka) - I_n'(nka)K_n(nka)}I_n'(nkb) \tag{14}$$

$$B_n = -kb\frac{I_n'(nka)K_n(nka) - I_n(nka)K_n'(nka)}{\kappa_m I_n(nka)K_n'(nka) - I_n'(nka)K_n(nka)} I_n'(nkb)$$
$$= -\frac{b}{na}\frac{1}{\kappa_m I_n(nka)K_n'(nka) - I_n'(nka)K_n(nka)} I_n'(nkb) \quad (15)$$

Therefore, the magnetic scalar potential $\phi_{1,iron}$ at z=0 due to the contribution of an axially symmetric iron yoke on the region 1 is expressed as follows,

$$\phi_{1,iron} = \frac{I}{\pi}\sum_{n=1}^{\infty}\frac{(\kappa_m - 1)K_n(nka)K_n'(nka)}{\kappa_m I_n(nka)K_n'(nka) - I_n'(nka)K_n(nka)} kbI_n'(nkb)I_n(nkr)\sin n\theta$$
$$= \frac{I}{\pi}\sum_{n=1}^{\infty}\frac{\kappa_m - 1}{\kappa_m - I_n'(nka)K_n(nka)/I_n(nka)K_n'(nka)}\frac{K_n(nka)}{I_n(nka)} kbI_n'(nkb)I_n(nkr)\sin n\theta \quad (16)$$

Especially, on the case of iron with the infinite permeability ($\kappa_m=\infty$), the above equation becomes simple,

$$\phi_{1,iron} = \frac{I}{\pi}\sum_{n=1}^{\infty}\frac{K_n(nka)}{I_n(nka)} kbI_n'(nkb)I_n(nkr)\sin n\theta \quad (17)$$

from the following equation,

$$\lim_{\kappa_m\to\infty}\frac{\kappa_m - 1}{\kappa_m - I_n'(nka)K_n(nka)/I_n(nka)K_n'(nka)} = 1 \quad (18)$$

On the other hand, on the inner surface of iron with the infinite permeability ($\kappa_m=\infty$), the simple boundary condition of $\phi_{1,coil} + \phi_{1,iron} = 0$ is used by Caspi for helical magnets. [2] Caspi has studied the more versatile situation of helical magnets by using the more complicated expressions. [2] This simple boundary condition can be applied for the system with the additional return current at origin, as remarked by Halbach. [3] Actually, on the case that a single helical current conductor together with the straight return current at origin,

$$\phi_1(r,\theta,z=0) = \phi_{1,coil}(r,\theta,z=0) + \phi_{1,return}(r,\theta,z=0) + \phi_{1,iron}(r,\theta,z=0) = 0 \quad (19)$$

$$-\frac{I}{2\pi}\theta-\frac{I}{\pi}kb\sum_{n=1}^{\infty}I_n'(nkb)K_n(nkr)\sin n\theta+\frac{I}{2\pi}\theta-\frac{I}{\pi}\sum_{n=1}^{\infty}A_n'I_n(nkr)\sin n\theta=0 \tag{20}$$

As a result, the following expression equivalent with Eq.(17) is obtained,

$$A_n'=-kb\frac{K_n(nka)}{I_n(nka)}I_n'(nkb) \tag{21}$$

The asymptotic forms for the following terms with the modified Bessel functions and their derivatives as k → 0 (L →∞) are as follows,[4]

$$\frac{I_n'(nka)K_n(nka)}{I_n(nka)K_n'(nka)}\approx -1 \tag{22}$$

$$\frac{K_n(nka)}{I_n(nka)}kbI_n'(nkb)I_n(nkr)\approx\frac{1}{2n}\left(\frac{r}{a^2/b}\right)^n \tag{23}$$

Then, it can be revealed that the magnetic scalar potential ϕ_{1i} results the potential on the case of the straight image current, as k → 0 (L →∞). [5,6,7]

$$\phi_{1,iron,straight}=\lim_{k\to 0}\phi_{1,iron}=\frac{I}{2\pi}\frac{\kappa_m-1}{\kappa_m+1}\sum_{n=1}^{\infty}\left(\frac{r}{a^2/b}\right)^n\frac{\sin n\theta}{n} \tag{24}$$

Similarly, the magnetic scalar potential ϕ_2 on the region 2, (r > a) is written as the following form,

$$\begin{aligned}\phi_2&=-\frac{I}{2\pi}\theta+\frac{I}{\pi}\sum_{n=1}^{\infty}\frac{1}{\kappa_m I_n(nka)K_n'(nka)-I_n'(nka)K_n(nka)}\frac{b}{na}I_n'(nkb)K_n(nkr)\sin n\theta\\&=-\frac{I}{2\pi}\theta+\frac{I}{\pi}\sum_{n=1}^{\infty}\frac{1}{\kappa_m-\frac{I_n'(nka)K_n(nka)}{I_n(nka)K_n'(nka)}}\frac{b}{na}\frac{I_n'(nkb)}{I_n(nka)K_n'(nka)}K_n(nkr)\sin n\theta\end{aligned} \tag{25}$$

The asymptotic form for the following term as k → 0 (L →∞) are as follows, [4]

$$\frac{b}{na}\frac{I_n'(nkb)}{I_n(nka)K_n'(nka)}K_n(nkr) \approx -\frac{1}{n}\left(\frac{b}{r}\right)^n \tag{26}$$

Then, it can also be revealed that the magnetic scalar potential ϕ_2 results the potential of the 2-dimensional case, as k $\rightarrow$ 0 (L $\rightarrow\infty$). [5,6,7]

$$\phi_{2,straight} = \lim_{k\to 0}\phi_2 = -\frac{I}{2\pi}\theta - \frac{I}{\pi}\sum_{n=1}^{\infty}\frac{1}{\kappa_m + 1}\left(\frac{b}{r}\right)^n \frac{\sin n\theta}{n} \tag{27}$$

Finally, on the case that a single helical current carrying conductor with a pitch length L (= 2π/k) is located at a point (r=b, $\theta=\varphi$) at the z=0 plane, the general form for the magnetic scalar potential $\phi_{1,iron}$ due to an axially symmetric iron yoke on the region 1 is expressed as follows,

$$\begin{aligned}\phi_{1,iron}(r,\theta,z) &= \frac{I}{\pi}\sum_{n=1}^{\infty}\left\{\frac{\kappa_m - 1}{\kappa_m - {I_n'(nka)K_n(nka)}/{I_n(nka)K_n'(nka)}}\right\} \\ &\times\frac{K_n(nka)}{I_n(nka)}kbI_n'(nkb)I_n(nkr)\sin[n(\theta-\varphi-kz)]\end{aligned} \tag{28}$$

Therefore, the general form for the magnetic scalar potential in region 1, (r < a) is expressed as a sum of Eq.(3) and Eq.(28) for the interior region, (r < b) of the helical coil or as a sum of Eq.(5) and Eq.(28) for the exterior region, (b < r < a) of the helical coil. Similarly, the general form for the magnetic scalar potential ϕ_2 on the region 2, (r > a) is expressed as follows,

$$\begin{aligned}\phi_2 &= -\frac{I}{2\pi}\theta \\ &+\frac{I}{\pi}\sum_{n=1}^{\infty}\frac{1}{\kappa_m - {I_n'(nka)K_n(nka)}/{I_n(nka)K_n'(nka)}}\frac{b}{na}\frac{I_n'(nkb)}{I_n(nka)K_n'(nka)}K_n(nkr)\sin[n(\theta-\varphi-kz)]\end{aligned} \tag{29}$$

Then, the field B can be calculated from the following equation,

$$\begin{cases}B_1 = -\mu_1\nabla\phi_1 = -\mu_0\nabla\phi_1 \\ B_2 = -\mu_2\nabla\phi_2 = -\kappa_m\mu_0\nabla\phi_2\end{cases} \tag{30}$$

Especially, the fields, $B_{1r,iron}$, $B_{1\theta,iron}$, $B_{1z,iron}$, due to the contribution of an axially symmetric iron yoke on the region 1 is expressed as follows,

$$\begin{cases} B_{1r,iron}(r,\theta,z) = \\ -\dfrac{\mu_0 I}{\pi} k^2 b \sum_{n=1}^{\infty} n \left\{ \dfrac{\kappa_m - 1}{\kappa_m - \frac{I_n'(nka)K_n(nka)}{I_n(nka)K_n'(nka)}} \right\} \dfrac{K_n(nka)}{I_n(nka)} I_n'(nkb) I_n'(nkr) \sin[n(\theta - \varphi - kz)] \\ B_{1\theta,iron}(r,\theta,z) = \\ -\dfrac{\mu_0 I}{\pi} kb \sum_{n=1}^{\infty} n \left\{ \dfrac{\kappa_m - 1}{\kappa_m - \frac{I_n'(nka)K_n(nka)}{I_n(nka)K_n'(nka)}} \right\} \dfrac{K_n(nka)}{I_n(nka)} I_n'(nkb) \dfrac{I_n(nkr)}{r} \cos[n(\theta - \varphi - kz)] \\ B_{1z,iron}(r,\theta,z) = \\ +\dfrac{\mu_0 I}{\pi} k^2 b \sum_{n=1}^{\infty} n \left\{ \dfrac{\kappa_m - 1}{\kappa_m - \frac{I_n'(nka)K_n(nka)}{I_n(nka)K_n'(nka)}} \right\} \dfrac{K_n(nka)}{I_n(nka)} I_n'(nkb) I_n(nkr) \cos[n(\theta - \varphi - kz)] \end{cases} \tag{31}$$

The qualitative difference between the interior fields of a single helical conductor, as shown in Figs. 1 and 2 due to a single helical conductor and an axially symmetric iron yoke comes from the existence of the first term independent on θ of the expression for B_z of Eq. (4), in comparison with $B_{1z,iron}$ of Eq. (31). Then, it is realized that the method of helical image currents is not applicable for the helical magnets with an axially symmetric iron yoke, though the difference becomes unclear with the cancellation of the first term due to the paired conductors comprising the dipole symmetry for the helical dipole magnets.

For the simple case that a single helical current conductor is placed inside a cylindrical hole in iron, with radius of a cylindrical hole in iron, a = 0.3 m, radius of helical line current, b = 0.25 m, relative permeability of iron, κ_m = 10, angle of helical line current at the z=0 plane, φ=0, current, I = 10^6 A, pitch length, L = 0.2 m, and k = 2π/L = 10π rad/m, as shown in Figs. 1 and 2, as an example, the vector plot of (B_x, B_y) at the z=0 plane, and the contour plot of H_z, is analytically calculated, as shown in Figs. 3 and 4, respectively. The fields calculated with Eqs. (4), (6), and (31) oscillates in the immediate neighborhood of the boundary of radius of helical line current (r = b) and radius of a cylindrical hole in iron (r = a), depending on the number of terms for summation. In Figs. 3 and 4, The calculated results based on the analytical expressions of Eqs. (4), (6), and (31) to N=50 for the double summations, as expressed in Eq. (39) of reference [1] (Cesàro's method) are plotted. With Cesàro's method of summation, however, the convergence is quite low. This means that the analytical method has some difficulties in the immediate neighborhood of the boundaries. In Fig. 3, the iron is represented with the

gray region, and the circular position of a single helical current conductor is also shown by the dashing line. On the contour plot of H_z, the white region corresponds to the high value, otherwise, the dark region corresponds to the low.

For this simple case, TOSCA is also applicable. [8] Actually, it can be confirmed that the analytically calculated results coincide with those numerically calculated by TOSCA for this simple case with the constant permeability for iron.

4 FIELD CALCULATION FOR HELICAL DIPOLE PROTOTYPE

4.1 Analytical expression of the magnetic field

As an extension of 2D magnetic field, the interior magnetic potential and field of helical dipole magnets with an infinite length can be expressed with the definition of the helical dipole reference field, $\tilde{B}_{ref}$, the helical normal and skew multipole coefficients, $\tilde{b}_n$ and $\tilde{a}_n$, the reference radius, r_0, in the following forms,

$$\phi_m(r,\theta,z) = -\frac{\tilde{B}_{ref} r_0}{\mu_0} \sum_{n=1}^{\infty} \frac{1}{n} n! \left(\frac{2}{nkr_0}\right)^n I_n(nkr)\left\{-\tilde{a}_n \cos[n(\theta - kz)] + \tilde{b}_n \sin[n(\theta - kz)]\right\} \quad (32)$$

$$\begin{cases} B_r(r,\theta,z) = -\mu_0 \dfrac{\partial \phi_m}{\partial r} \\ = \tilde{B}_{ref} r_0 \displaystyle\sum_{n=1}^{\infty} n! \left(\frac{2}{nkr_0}\right)^n k I_n'(nkr)\left\{-\tilde{a}_n \cos[n(\theta - kz)] + \tilde{b}_n \sin[n(\theta - kz)]\right\} \\ B_\theta(r,\theta,z) = -\mu_0 \dfrac{\partial \phi_m}{r\partial \theta} \\ = \tilde{B}_{ref} r_0 \displaystyle\sum_{n=1}^{\infty} n! \left(\frac{2}{nkr_0}\right)^n \frac{I_n(nkr)}{r}\left\{\tilde{a}_n \sin[n(\theta - kz)] + \tilde{b}_n \cos[n(\theta - kz)]\right\} \\ B_z(r,\theta,z) = -\mu_0 \dfrac{\partial \phi_m}{\partial z} \\ = \tilde{B}_{ref} r_0 \displaystyle\sum_{n=1}^{\infty} (-k) n! \left(\frac{2}{nkr_0}\right)^n I_n(nkr)\left\{\tilde{a}_n \sin[n(\theta - kz)] + \tilde{b}_n \cos[n(\theta - kz)]\right\} \end{cases} \quad (33)$$

The interior magnetic fields of helical dipole magnets with an infinite length can easily be derived from the summation of many helical line currents. Then, the helical normal and skew multipoles for the helical dipole magnet with m helical line currents with current I_j, radius b_j, and angle φ_j, (j=1,2 ..,m) can be expressed with the definition of $\tilde{b}_1$=1 (i.e., $\tilde{B}_{ref} = \tilde{B}_1$) in the following forms. Each multipole component is expressed as the sum of the contributions due to coil and iron,

for the dipole component (n=1),

$$\tilde{B}_{ref} = \tilde{B}_1 = \tilde{B}_{coil,1} + \tilde{B}_{iron,1} \tag{34}$$

where

$$\tilde{B}_{coil,1} = \frac{\mu_0}{2\pi} k^2 \sum_{j=1}^{m} I_j b_j K_1'(kb_j) \cos\varphi_j \tag{35}$$

and

$$\tilde{B}_{iron,1} = -\frac{\mu_0}{2\pi} k^2 \left\{ \frac{\kappa_m - 1}{\kappa_m - {I_1'(ka)K_1(ka)}/{I_1(ka)K_1'(ka)}} \right\} \sum_{j=1}^{m} I_j \frac{K_1(ka)}{I_1(ka)} b_j I_1'(kb_j) \cos\varphi_j \tag{36}$$

for the normal multipole components,

$$\tilde{B}_n = \tilde{B}_{ref} \tilde{b}_n = \tilde{B}_{coil,n} + \tilde{B}_{iron,n} \tag{37}$$

where

$$\tilde{B}_{coil,n} = \frac{\mu_0}{\pi} \frac{1}{2^n (n-1)! r_0} (nkr_0)^n k \sum_{j=1}^{m} I_j b_j K_n'(nkb_j) \cos n\varphi_j \tag{38}$$

and

$$\begin{aligned} \tilde{B}_{iron,n} = & -\frac{\mu_0}{\pi} \frac{1}{2^n (n-1)! r_0} (nkr_0)^n k \left\{ \frac{\kappa_m - 1}{\kappa_m - {I_n'(nka)K_n(nka)}/{I_n(nka)K_n'(nka)}} \right\} \\ & \times \sum_{j=1}^{m} I_j \frac{K_n(nka)}{I_n(nka)} b_j I_n'(nkb_j) \cos n\varphi_j \end{aligned} \tag{39}$$

for the skew multipole components,

$$\tilde{A}_n = \tilde{B}_{ref} \tilde{a}_n = \tilde{A}_{coil,n} + \tilde{A}_{iron,n} \tag{40}$$

where

$$\tilde{A}_{coil,n} = \frac{\mu_0}{\pi} \frac{1}{2^n (n-1)! r_0} (nkr_0)^n k \sum_{j=1}^{m} I_j b_j K_n'(nkb_j) \sin n\varphi_j \tag{41}$$

and

$$\tilde{A}_{iron,n} = -\frac{\mu_0}{\pi} \frac{1}{2^n (n-1)! r_0} (nkr_0)^n k \left\{ \frac{\kappa_m - 1}{\kappa_m - I_n'(nka) K_n(nka) / I_n(nka) K_n'(nka)} \right\} \times \sum_{j=1}^{m} I_j \frac{K_n(nka)}{I_n(nka)} b_j I_n'(nkb_j) \sin n\varphi_j \tag{42}$$

In the case of the iron yoke with the infinite permeability ($\kappa_m = \infty$), the above expressions of Eqs. (31), (34), and (37), become simple with Eq. (18).

4.2 Field calculation for a helical dipole prototype for RHIC

For the R & D of superconducting helical dipoles used in 'Siberian Snake' and 'Spin Rotator' for RHIC, the magnetic structure of the slotted helical dipole prototype with the half-length has been extensively studied. [9] The main parameters of the slotted helical dipole prototype with the half-length for RHIC are listed in Table 1 of reference [1]. The cross section of the slotted helical dipole prototype with the half-length for RHIC is also shown in Fig. 12 of reference [1].

The analytically and numerically calculated and measured results of the multipoles for a single current of 200 A are listed in Table 1, together with the newly calculated results. Table 1 is revised from Table 2 of reference [1]. In Table 1, the reference radius is defined as r_0 = 31 mm, and $\tilde{B}_{ref,coil}$ (= $\tilde{B}_{coil,1}$ shown in Eqs. (34) and (35)) is the contribution due to the helical coil for the helical dipole reference field. The analytically calculated results for the interior magnetic field of the helical dipole are obtained from the summation for the field contribution of all 1728 (= 864 × 2) turns or 864 sets of four helical line currents. The measured data is the results by the rotating coil of the tangential winding. The calculated results by TOSCA are shown with three different values which derived from the distributions of B_r, B_θ, or B_z, respectively, on the circle of of 31 mm (reference radius) of the middle plane of magnet.

On the previous calculation, the contribution of an axially symmetric iron yoke or the effect of the iron yoke is approximately calculated with the simple assumption that the helical image current is the same with the case of the straight current for the position (or radius) and the intensity of the image current. This calculated results are referred as the

old analytical calculation (old analytical) in Table 1. The contribution of an axially symmetric iron yoke is newly calculated, using Eqs. (36), (39), and (42) derived from Eq. (31), with the assumption of the infinite permeability ($\kappa_m=\infty$), based on the rigorous treatment of the potential problem, while the contribution of the helical coil is calculated, using Eqs. (35), (38), and (41) derived from Eq. (4), similarly with the previous calculation. The agreement with the numerical calculation by TOSCA and the measured result is greatly improved, as shown in Table 1. This newly calculated results are referred as the new analytical calculation (new analytical) in Table 1. On this analytical calculation, the length of the magnet is assumed to be infinite. On the other hand, the numerical calculation by TOSCA is made for the geometry of the actual magnet with finite length and coil ends, and for the iron yoke with the nonlinear B-H characteristics.

From the comparison among the analytically and numerically calculated and measured results, listed in Table 1, firstly, on the numerical calculation by TOSCA, it seems reasonable that there are small differences among each multipoles, deviated from the ideal distribution with identical or common multipole coefficients for each field components, as shown in Eq. (33). Secondly, from the existence of the forbidden multipoles (quadrupole, octupole, etc.) and the skew multipoles on the measured results, it implies that the actual geometry of this helical dipole prototype deviates from the perfect dipole symmetry. Actually, on the numerical calculation by TOSCA for the helical magnet with the perfect dipole symmetry, the values of the forbidden multipoles (quadrupole, octupole, etc.) and the skew multipoles are quite small.

The comparison among the analytical calculations of the new or revised (solid) and the old (dashing) results, and measured results by rotating coils (line with dots) for the current dependence of the helical dipole reference field $\tilde{B}_{ref}$ is shown in Fig. 5. The measured data contain the results by three rotating coils, dipole #1, dipole #2, and tangential windings. [10] The difference among the results of the helical dipole reference field $\tilde{B}_{ref}$ by three rotating coils is quite small, as shown in Fig. 5. Contour plot of the vertical field component, B_y, derived (or synthesized) from the new analytical calculation up to 18-pole at I = 200 A listed in Table 1, is revised, as shown in Fig. 6, instead of Fig. 13 of reference [1]. The difference between both the new and old contour plots looks quite small, as speculated from the small difference between 2 calculated results for the helical normal multipole coefficients $\tilde{b}_n$.

5 CONCLUSION

For the analytical field calculation for the helical magnets with an axially symmetric iron yoke, the 3-dimensoinal potential problem for the case that a single helical current

carrying conductor is placed inside a cylindrical hole in iron is rigorously solved. As a result, it is realized that the method of image currents is not applicable for the helical magnets, even qualitatively.

On the low excitation without the iron saturation, the obtained analytical expressions for the contribution due to an iron yoke are applied for the field calculation of the slotted helical dipole prototype with the half-length for RHIC, with good agreement among the other numerical calculations and measured results.

Furthermore, it is expected that this analytical method can be extended for the fundamental field calculation of electric machines with a skewed rotor, which basically consist of helical current conductors lying in the air gap between concentric iron cylinders.

ACKNOWLEDGMENTS

The authors are indebted for helpful discussions and comments to the BNL/RIKEN RHIC spin accelerator group.

References

[1] T. Tominaka, M. Okamura, and T. Katayama, "Analytical Field Calculation of Helical Coils", Nucl. Instr. & Meth. A 459 (2001) pp.398-411.
[2] S. Caspi, "Magnetic Field Components in a Sinusoidally Varying Helical Wiggler", SC-MAG-464, LBL-35928, (1994).
[3] K. Halbach, "Fields and First Order Perturbation Effects in Two-Dimensional Conductor Dominated Magnets", Nucl. Instr. and Meth. 78, pp.185-198 (1970).
[4] M. Abramowitz and I. A. Stegun (eds.), "Handbook of Mathematical Functions", Dover, pp.374-376 (1970).
[5] B. Hague, "The Principles of Electromagnetism Applied to Electrical Machines", Dover, p.124 (1962).
[6] M. Stafl, "Electrodynamics of Electrical Machines", Academia, p.84 (1967).
[7] W. R. Smythe, "Static and Dynamic Electricity", McGraw-Hill, p.310 (1968).
[8] Vector Fields Limited, Oxford, UK.
[9] M. Okamura et al., "Half Length Model of a Siberian Snake Magnet for RHIC", Nucl. Instr. & Meth. A 452 (2000) pp.53-60.
[10] T. Tominaka, M. Okamura, and T. Katayama, "Field Distributions of the Slotted Helical Dipole Prototypes with the Half and Full-Length", AGS/RHIC/SN No.74, July 22, (1998).

Table Captions

Table 1. Helical multipole coefficients (10^{-4}) for the half-length helical dipole prototype, at I = 200 A.

Table 1

n	Pole	$\tilde{b}_n$ (old analytical)	$\tilde{b}_n$ (new analytical)	$\tilde{b}_n$ from B_r, (TOSCA)	$\tilde{b}_n$ from B_θ, (TOSCA)	$\tilde{b}_n$ from B_z, (TOSCA)	$\tilde{b}_n$ (measured)	$\tilde{a}_n$
$\tilde{B}_{ref}$ (T)		2.81	2.72	2.714	2.714	2.713	2.72	
$\tilde{B}_{ref,coil}$ (T)		1.75	1.75	-	-	-	-	
2	quadrupole	-	-	-	-	-	1.2	- 0.41
3	sextupole	- 49.3	- 50.8	- 52.5	- 52.4	- 53.0	- 63.2	- 0.26
4	octupole	-	-	-	-	-	2.3	0.03
5	decapole	5.5	5.7	5.9	6.0	6.1	9.7	2.4
6	dodecapole	-	-	-	-	-	- 0.54	- 1.2
7	14 - pole	0.29	0.29	0.27	0.29	0.32	3.3	7.3
8	16 - pole	-	-	-	-	-	0.51	- 4.0
9	18 - pole	- 7.6	- 7.8	- 7.8	- 7.8	- 7.8	- 19.7	1.6
10	20 - pole	-	-	-	-	-	20.5	6.9

Figure captions

Fig. 1. Schematic view of a single helical coil placed inside a cylindrical hole in iron.

Fig. 2. Cross section of a single helical coil placed inside a cylindrical hole in iron (z=0).

Fig. 3. Vector plot of (B_x, B_y) at z=0 analytically calculated to N=50 (Cesàro's method).

Fig. 4. Contour plot of H_z at z=0 analytically calculated to N=50 (Cesàro's method).

Fig. 3. Comparison among the new analytical calculation (solid), the old analytical (dashing), and measured results by rotating coils (line with dots) for the current dependence of the helical dipole reference field $\tilde{B}_{ref}$.

Fig. 4. Contour plot of B_y at I = 200 A (new analytical calculation).

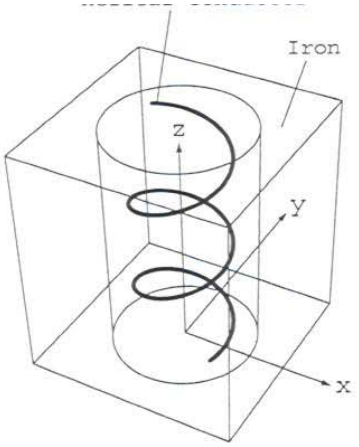

Fig. 1

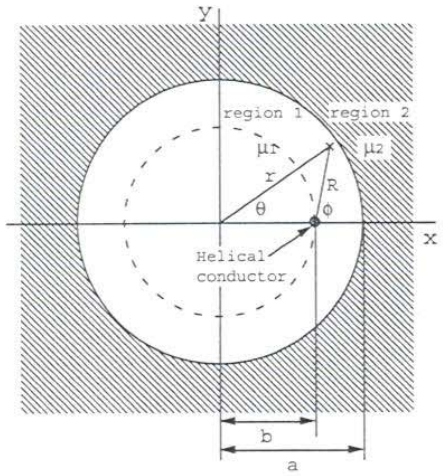

Fig. 2

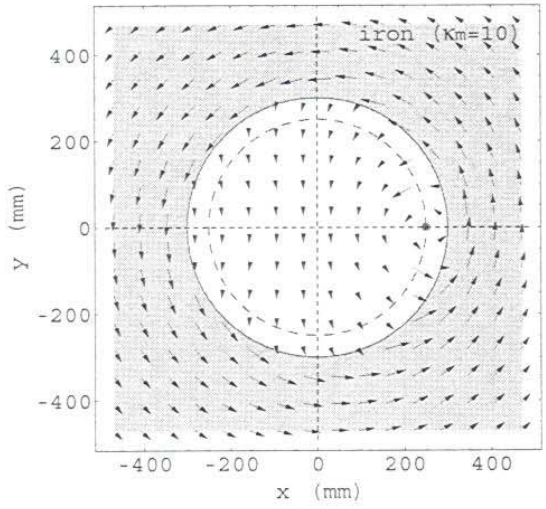

Fig. 3

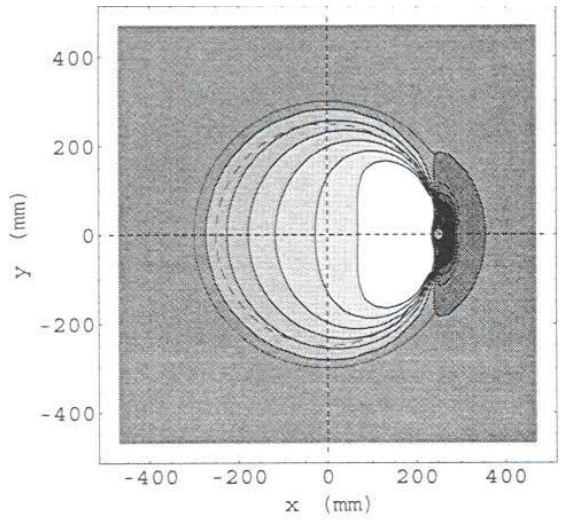

Fig. 4

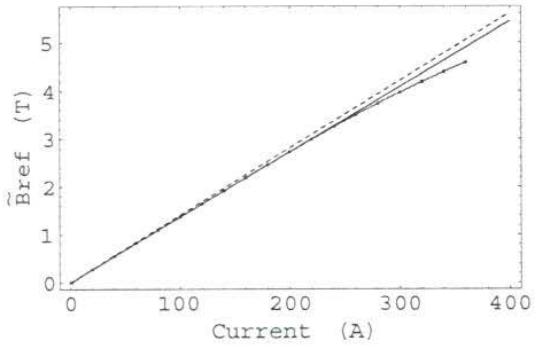

Fig. 5

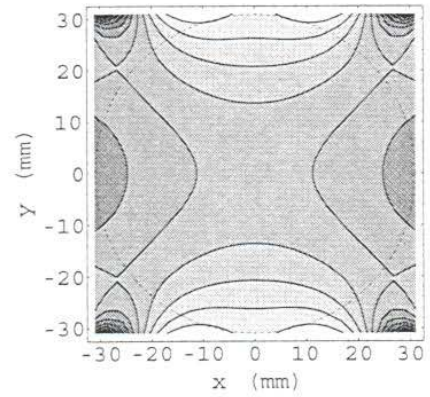

Fig. 6